

# Critical phenomena and quantum discord of quantum antiferromagnetic Heisenberg model on diamond-type hierarchical lattices

Pan-Pan Zhang<sup>1</sup>, Zhong-Yang Gao<sup>2</sup>, Yu-Liang Xu<sup>1</sup>, Chun-Yang Wang<sup>1</sup> and Xiang-Mu Kong<sup>1,2\*</sup>

<sup>1</sup>*School of Physics and Optoelectronic Engineering,*

*Ludong University, Yantai 264025, China*

<sup>2</sup>*College of physics and Engineering,*

*Qufu Normal University, Qufu 273165, China*

(Dated: February 25, 2021)

## Abstract

The anisotropic spin-1/2 antiferromagnetic Heisenberg systems are studied on three typical diamond-type hierarchical lattices (systems A, B and C) with fractal dimensions  $d_f = 1.63$ , 2 and 2.58, respectively. For system A, using the real-space renormalization group approach, we calculate the phase diagram, the critical exponent and quantum discord, and find that there exists a reentrant behavior in the phase diagram. We also find that the quantum discord reaches its maximum at  $T = 0$  and the thermal quantum discord decreases with the increase of  $L$ , and it is almost zero at  $L \geq 30$ . No matter how large the size of system is, quantum discord will change to 0 when anisotropic parameter  $\Delta = 1$ . For systems B and C, using the equivalent transformation and the real-space renormalization group method, we obtain phase diagrams and find that: the Néel temperature tends to zero in the isotropic Heisenberg limit on  $d_f = 2$  system; there exists a phase transition in the isotropic Heisenberg model on system C. By studying quantum discord, we find that there is a certain degree of twist of the relation curve between quantum discord and  $T$  when  $\Delta = 0$ . Moreover, as an example, we discuss the quantum effect in system A, which can be responsible for the existence of the reentrant behavior in the phase diagram.

PACS numbers:

---

\*Corresponding author. E-mail address: kongxm668@163.com (X.-M. Kong).

## I. INTRODUCTION

The research on fractal lattice system is always a hot topic because of its unique structure, there are already massive researches about classical systems[1–3], but the research work about quantum system are relatively less[4, 5]. In 2003, de Sousa et al. studied the phase diagram of the two-dimensional quantum spin anisotropic Heisenberg model[5]. Recently, Sierpinski fractal materials have been synthesized in the laboratory[6]. It is necessary to further study the fractal lattice.

As an important parameter to describe phase transition, the critical temperature has an important effect on critical behavior. The research shows that the critical temperature  $T_c = 0$  and  $T_c > 0$  for the isotropic ferromagnetic (F) Heisenberg system on diamond-type hierarchical (DH) lattice with fractal dimensions  $d_f = 2$  and  $d_f = 3$ , respectively[5, 7, 8], but antiferromagnetic (AF) Heisenberg systems need further study. Various renormalization group approaches[9–12], Green’s function technique[13, 14], spin-wave theory [15] and Monte Carlo method [16, 17] have been applied to study the quantum AF Heisenberg systems. de Sousa et al. calculated the phase diagram of the AF Heisenberg model by the mean-field RG approach and found that the AF Néel temperature  $T_N < T_c$  for 2D lattices and  $T_N > T_c$  for 3D lattices [12, 18]. However, results from spin-wave theory and Green’s function technique on the isotropic Heisenberg model obtained  $T_N = T_c$  for 2D and 3D lattices in AF Heisenberg system[14, 15, 19, 20]. Quantum Monte Carlo results indicate that an ordered low temperature phase is obtained even at much smaller anisotropies  $\Delta \sim 10^{-3}$  for 2D lattices in AF Heisenberg system[16, 21]. From these results, we can see that the situation for fractal lattice system is still unclear and it is worth our further study.

Quantum correlation, as an important quantum resource, has been applied to quantum communication, quantum teleportation, and quantum computation, etc[22, 23]. Quantum correlation contains more quantum information than quantum entanglement which is one particular quantum correlation[24, 25]. The quantum discord (QD) which captures nonclassical correlation even without entanglement is proved as an effective measure for all aspects of quantum correlation[26, 27]. As a wider class of measures than entanglement, QD has become an active research topic over the past few years[28–30], which has important application value in quantum information processing, quantum dynamics and even biophysics[31–34]. But, it isn’t difficult to find that the present studies have focused on the one-dimensional

spin chain, the studies of fractal lattices are less[29, 35].

In this work, we investigate the phase diagrams and QD of the anisotropic AF Heisenberg model on three kinds of diamond-type hierarchical lattices (systems A, B and C), with fractal dimensions  $d_f = 1.63, 2$  and  $2.58$ , respectively, which is shown in Fig. 1. Using the real-space RG method straightforwardly, we study the phase diagram, some critical behaviors and quantum correlations under different temperature and the anisotropic parameters on system A. For systems B and C, we apply an effective combination method of the equivalent transformation (ET) and the real-space RG method, which has been used for classical systems in Ref. [3] but for quantum systems this is done for the first time as far as we know.

The structure of this paper is organized as follows. In Sec. II we outline the method and the critical behaviors for system A. In Sec. III the method and the critical behaviors are presented for systems B and C. Sec. IV discusses the quantum correlations for the three lattices. In Sec. V the analyses of the quantum effect is discussed. The summary is given in the the last section.

## II. THE METHOD AND CRITICAL BEHAVIORS FOR SYSTEM A

The anisotropic spin-1/2 Heisenberg model is described by the effective Hamiltonian

$$H = K \sum_{\langle ij \rangle} [(1 - \Delta)(\sigma_i^x \sigma_j^x + \sigma_i^y \sigma_j^y) + \sigma_i^z \sigma_j^z], \quad (1)$$

where  $K = J/k_B T$ ,  $J$  is the exchange coupling constant (with  $J < 0$  and  $J > 0$  correspond to AF model and ferromagnetic (F) one, respectively),  $k_B$  is the Boltzmann constant,  $T$  is the temperature,  $\langle ij \rangle$  denotes nearest-neighbor spin pairs,  $\Delta \in [0, 1]$  is the anisotropic parameter, and  $\sigma_i^\alpha$  ( $\alpha = x, y, z$ ) are components of a spin-1/2 operator at site  $i$ . Note that, as particular cases, the Hamiltonian (1) describes the Ising model ( $\Delta=1$ ), isotropic Heisenberg model ( $\Delta=0$ ) and XY model ( $\Delta=-\infty$ ), respectively.

In this section, using the real-space RG method[4, 36], we study the phase diagram and some critical behaviors of the anisotropic Heisenberg model on the DH lattice A. Such kind of lattices are constructed in an iterative manner, starting from a two-point lattice[37, 38] (Fig. 1). We take out the generator from system A to perform the RG transformation, which is shown in Fig. 2(a). As we can see, after summation of the internal spins, the generator (Fig. 2(a1)) is transformed into a new structure, which contains  $\sigma_1$  and  $\sigma_2$ , joined

by a single bond (Fig. 2(a2)). This procedure can be described as

$$\exp(H'_{12}) = \text{Tr}_{3456} \exp(H_{123456}), \quad (2)$$

where

$$H'_{12} = K_s[(1 - \Delta_s)(\sigma_1^x \sigma_2^x + \sigma_1^y \sigma_2^y) + \sigma_1^z \sigma_2^z] + K_0$$

and

$$\begin{aligned} H_{123456} = & K(1 - \Delta)[(\sigma_1^x \sigma_3^x + \sigma_1^y \sigma_3^y) + (\sigma_1^x \sigma_6^x + \sigma_1^y \sigma_6^y) + (\sigma_3^x \sigma_5^x + \sigma_3^y \sigma_5^y) \\ & + (\sigma_4^x \sigma_6^x + \sigma_4^y \sigma_6^y) + (\sigma_2^x \sigma_5^x + \sigma_2^y \sigma_5^y) + (\sigma_2^x \sigma_4^x + \sigma_2^y \sigma_4^y)] \\ & + K(\sigma_1^z \sigma_3^z + \sigma_1^z \sigma_6^z + \sigma_3^z \sigma_5^z + \sigma_4^z \sigma_6^z + \sigma_2^z \sigma_5^z + \sigma_2^z \sigma_4^z) \end{aligned}$$

are the Hamiltonians of the renormalized two-site cluster and of the six-site cluster (see Fig. 2(a)), respectively.  $\text{Tr}_{3456}$  denotes a partial trace over the internal  $\sigma_i (i = 3, 4, 5, 6)$ . To make Eq. (2) possible, an additional constant  $K_0$  has been included in  $H'_{12}$ . The RG recursion relations between the renormalized parameters  $(K_s, \Delta_s)$  and the original parameters  $(K, \Delta)$  are determined by Eq. (2). Notice that the noncommutativity between the Hamiltonians of the neighboring clusters is neglected, and therefore our results are approximations, and a discussion for this approximation will be presented in Sec. V.

In order to calculate the partial trace in Eq. (2), we expand  $\exp(H'_{12})$  as

$$\exp(H'_{12}) = a' + b'_{12}(\sigma_1^x \sigma_2^x + \sigma_1^y \sigma_2^y) + c'_{12} \sigma_1^z \sigma_2^z, \quad (3)$$

where  $a'$ ,  $b'_{12}$  and  $c'_{12}$  are functions of  $K'$ ,  $\Delta'$  and  $K_0$ . In the representation of the direct product of  $\sigma_1^z$  and  $\sigma_2^z$ , both the left-hand side and the right-hand side of Eq. (3) can be expressed as  $4 \times 4$  matrixes and we finally obtain

$$\exp(4K_s) = \frac{(a' + c'_{12})^2}{(a' - c'_{12})^2 - 16b_{12}^2}, \quad (4)$$

$$\exp(4K_s \Delta_s) = \frac{(a' + c'_{12})^2}{(a' + 4b'_{12} - c'_{12})^2} \quad (5)$$

and

$$\exp(K_0) = \frac{a' + c'_{12}}{\exp(K_s)}. \quad (6)$$

Similarly, we expand  $\exp(H_{123456})$  as

$$\begin{aligned} \exp(H_{123456}) = & a + \sum_{\langle i < j \rangle} [b_{ij} (\sigma_i^x \sigma_j^x + \sigma_i^y \sigma_j^y) + c_{ij} \sigma_i^z \sigma_j^z] \\ & + \sum_{\langle i < j \rangle \neq \langle k < l \rangle} A + \sum_{\langle i < j \rangle \neq \langle k < l \rangle \neq \langle m < n \rangle} B + r \sigma_1^z \sigma_2^z \sigma_3^z \sigma_4^z \sigma_5^z \sigma_6^z, \end{aligned} \quad (7)$$

in which

$$A = e_{ij,kl}(\sigma_i^x \sigma_j^x + \sigma_i^y \sigma_j^y)(\sigma_k^x \sigma_l^x + \sigma_k^y \sigma_l^y) + d_{ij,kl}(\sigma_i^x \sigma_j^x + \sigma_i^y \sigma_j^y)\sigma_k^z \sigma_l^z + f_{ij,kl}\sigma_i^z \sigma_j^z \sigma_k^z \sigma_l^z$$

and

$$B = g_{ij,kl,mn}(\sigma_i^x \sigma_j^x + \sigma_i^y \sigma_j^y)\sigma_k^z \sigma_l^z \sigma_m^z \sigma_n^z + p_{ij,kl,mn}(\sigma_i^x \sigma_j^x + \sigma_i^y \sigma_j^y)(\sigma_k^x \sigma_l^x + \sigma_k^y \sigma_l^y)\sigma_m^z \sigma_n^z \\ + q_{ij,kl,mn}(\sigma_i^x \sigma_j^x + \sigma_i^y \sigma_j^y)(\sigma_k^x \sigma_l^x + \sigma_k^y \sigma_l^y)(\sigma_m^x \sigma_n^x + \sigma_m^y \sigma_n^y),$$

where  $a$ ,  $\{b_{ij}\}$ ,  $\{c_{ij}\}$ ,  $\dots$   $\{q_{ij,kl,mn}\}$  and  $r$  depend on  $K$  and  $\Delta$ . From Eqs. (2), (3) and (7), it can be obtained that  $a' = 16a$ ,  $b'_{12} = 16b_{12}$ , and  $c'_{12} = 16c_{12}$ , and the recursion relations becomes

$$\exp(4K_s) = \frac{(a + c_{12})^2}{(a - c_{12})^2 - 4b_{12}^2}, \quad (8)$$

$$\exp(4K_s \Delta_s) = \frac{(a + c_{12})^2}{(a + 2b_{12} - c_{12})^2}. \quad (9)$$

By numerically iterating Eqs. (8) and (9), we obtain the AF phase diagram which is shown in Fig. 3. The inset shows the critical curve of the F system in Fig. 3 for comparison. We can see that there exists two phases, namely, an ordered phase and a disordered one characterized by fully stable fixed points  $(\infty, 1)$  and  $(0, 1)$ , respectively. There are two unstable fixed points at  $(0.94, 1)$  and  $(0, 0)$ , corresponding to the Ising and the isotropic Heisenberg model, respectively. The Ising fixed point of the F system is the same as that of the AF system. At the Ising fixed point, we obtain the correlation length critical exponent

$$\nu = \frac{\ln b}{\ln \lambda} = 1.779, \quad (10)$$

where  $b = 3$  is the scaling factor and  $\lambda \equiv (\partial K_s / \partial K) |_{\Delta=1, K=0.94}$ . At the isotropic Heisenberg fixed point of the F model, we obtain  $\nu = \infty$  which is consistent with the exact result [39]. For the AF model, the phase diagram is different from the F one: the transition line goes to zero at a value of  $\Delta_c = 0.703$ . Moreover, we find a reentrant behavior in the phase diagram. This fact is usually due to the quantum fluctuation which is related to the critical temperature and the anisotropy parameter and we will discuss it in Sec. V. Furthermore, we also calculate the critical behavior of this system when  $T \rightarrow 0$ . It is found that the critical temperature behaves as

$$T_c \sim \Delta \quad (11)$$

for the F case (Fig. 4(a)), and the Néel temperature  $T_N$  behaves as

$$T_N \sim \ln(\Delta_c - \Delta) \quad (12)$$

near  $\Delta_c = 0.703$  (Fig. 4(b)).

### III. THE METHOD AND CRITICAL BEHAVIORS FOR SYSTEMS B AND C

In this section, we use an effective combination method of the equivalent transformation (ET) and the real-space RG method to the AF Heisenberg model on systems B and C, which has been used for classical systems in Ref. [3] but for quantum systems this is done for the first time as far as we know. As we can see, Fig. 2(b) has antiferromagnetic interactions ( $K < 0$ ) and after the ET, it has ferromagnetic interactions ( $K' > 0$ ). Therefore, we can obtain the critical condition of an AF system if we know that of the equivalent system with ferromagnetic couplings. This method contains three steps (see Fig. 2(b)): (1) The ET technique is used to transform the AF system into an equivalent F one and the ET equations are obtained. (2) By numerically iterating the RG recursion equations of the equivalent F system, the critical points can be obtained. (3) The results obtained from the second step are substituted into the ET equations in the first step and the AF phase diagram can be obtained.

In the following, we give the calculation procedure of the AF Heisenberg model on system B. To construct the ET equations, we transform the cluster of Fig. 2(b1) (which contains four  $\sigma_i$  ( $i = 1, 2, 3, 4$ )) into Fig. 2(b2) (the cluster contains two spins-1 and 2). Following the same steps as in Sec. II, we can obtain the ET equations in the same form as Eqs. (4), (5) and (6), as well as the  $16 \times 16$  matrix  $\exp(H_{1234})$

$$\begin{aligned} \exp(H_{1234}) = & a + \sum_{i < j} [b_{ij}(\sigma_i^x \sigma_j^x + \sigma_i^y \sigma_j^y) + c_{ij} \sigma_i^z \sigma_j^z] \\ & + \sum_{(i < j) \neq (k < l)} d_{ij,kl} (\sigma_i^x \sigma_j^x + \sigma_i^y \sigma_j^y) \sigma_k^z \sigma_l^z \\ & + \sum_{(i < j) \neq (k < l)} e_{ij,kl} (\sigma_i^x \sigma_j^x + \sigma_i^y \sigma_j^y) (\sigma_k^x \sigma_l^x + \sigma_k^y \sigma_l^y) \\ & + f \sigma_1^z \sigma_2^z \sigma_3^z \sigma_4^z, \end{aligned} \quad (13)$$

where  $a$ ,  $\{b_{ij}\}$ ,  $\{c_{ij}\}$ ,  $\{d_{ij,kl}\}$ ,  $\{e_{ij,kl}\}$  and  $f$  are functions of  $K$  and  $\Delta$ . Furthermore, after some calculus as in Sec. II, it is obtained that  $a' = 4a$ ,  $b'_{12} = 4b_{12}$  and  $c'_{12} = 4c_{12}$ , and we

finally obtain the ET equations as

$$\exp(4K') = \frac{(a + c_{12})^2}{(a - c_{12})^2 - 4b_{12}^2}, \quad (14)$$

$$\exp(4K'\Delta') = \frac{(a + c_{12})^2}{(a + 2b_{12} - c_{12})^2}, \quad (15)$$

in which  $a$ ,  $b_{12}$ ,  $c_{12}$  are functions of  $K$  and  $\Delta$  and the equivalent system has ferromagnetic interactions  $K' > 0$ . For the equivalent ferromagnetic system, we obtain the RG recursion relations in the same form as Eqs. (14) and (15)

$$\exp(4K'') = \frac{(a + c_{12})^2}{(a - c_{12})^2 - 4b_{12}^2}, \quad (16)$$

$$\exp(4K''\Delta'') = \frac{(a + c_{12})^2}{(a + 2b_{12} - c_{12})^2}, \quad (17)$$

where  $a$ ,  $b_{12}$ ,  $c_{12}$  are functions of  $K'$  and  $\Delta'$ . Then, we substitute  $K'$  and  $\Delta'$  which are obtained by numerically iterating the ferromagnetic RG equations (16) and (17) into Eqs. (14) and (15), and finally get the phase diagram of the AF system.

Using the same procedure, we calculate the phase diagram of system C. However, the analytical expressions of the right-hand side of the ET equations of this system are difficult to calculate. In order to get the expressions, we express  $\exp(H_{12345})$  approximately as

$$\exp(H_{12345}) \approx 1 + H_{12345} + \frac{H_{12345}^2}{2!} + \dots + \frac{H_{12345}^{11}}{11!}, \quad (18)$$

in which we adopt the first twelve terms for convenient calculation.

Fig. 5 shows the phase diagram of systems B and C in  $(k_B T/|J|, \Delta)$  space. The AF critical line of system A is also depicted for comparison. There are two unstable fixed points for system B at (1.64, 1) and (0, 0) (for system C at (2.77, 1) and (2.06, 0)), corresponding to the Ising fixed point and the isotropic Heisenberg fixed point, respectively. The Ising fixed points (1.64, 1) and (2.77, 1) are the attractors of all  $\Delta \neq 0$  points in the critical lines. Physically, this indicates that the critical behavior along the lines are the same as that of the Ising model. Moreover, from Fig. 5, we find that:

- (1) For low-dimensional system A, there exists a reentrant behavior in the phase diagram.
- (2) For 2D system B, the Néel temperature tends to zero when decreasing  $\Delta$ .
- (3) For higher-dimensional system C, there exists phase transition in the isotropic Heisenberg limit  $\Delta = 0$ .

Which is in accordance with the previous quantum Monte Carlo[16, 21, 40, 41] and mean field renormalization group[11, 12, 18, 42] results. From our results, we can see that as the value of  $d_f$  increases the phase transition will present on the isotropic Heisenberg limit and as the value of  $d_f$  decreases the reentrant behavior will appear, and 2D maybe the critical dimension. We consider this phenomena to be the case for different fractal dimensions and the quantum effects which will be discussed in Sec. V. Moreover, we also calculate the critical behavior when  $T \rightarrow 0$  and obtain the following law for system B:

$$T_N \sim \frac{1}{\ln \Delta}, \quad (19)$$

the critical temperature behaves is shown in Fig. 6.

#### IV. THE QUANTUM CORRELATIONS FOR THE THREE LATTICES

In this section, we study the QD between two non-nearest-neighbor end spins of AF Heisenberg model in three diamond-type hierarchical lattices at finite temperatures and discuss the relations of QD with temperature and anisotropic parameter. It is widely accepted that quantum mutual information is a measure of the total correlation contained in a composite quantum system which includes classical and quantum correlations[43, 44]. We want to get quantum correlation by subtracting classical correlation from quantum mutual information. As a common representation of quantum correlation, QD captures nonclassical correlation even without entanglement. For a quantum state  $\rho_{12}$  of the composite system containing subsystems 1 and 2, the QD[29, 45] is defined as

$$D(\rho_{12}) = I(\rho_{12}) - C(\rho_{12}),$$

where  $I(\rho_{12})$  is the quantum mutual information and  $C(\rho_{12})$  is the classical correlation. Because the density matrix  $\rho$  of two spins in AF Heisenberg model exhibits an X structure, it is called X state, as

$$\rho_{12} = \begin{pmatrix} a_{11} & 0 & 0 & a_{14} \\ 0 & a_{22} & a_{23} & 0 \\ 0 & a_{32} & a_{33} & 0 \\ a_{41} & 0 & 0 & a_{44} \end{pmatrix},$$



where

$$\begin{aligned}
a_{11} &= a_{44} = \frac{e^k}{2e^k + e^{k(2\Delta-3)} + e^{k(1-2\Delta)}}, \\
a_{14} &= a_{41} = 0, \\
a_{22} &= a_{33} = \frac{e^k(1-2\Delta) + e^{k(2\Delta-3)}}{2(2e^k + e^{k(2\Delta-3)} + e^{k(1-2\Delta)})}, \\
a_{23} &= a_{32} = \frac{e^k(1-2\Delta) - e^{k(2\Delta-3)}}{2(2e^k + e^{k(2\Delta-3)} + e^{k(1-2\Delta)})}.
\end{aligned}$$

For two-qubit X state, there are some effective numerical and analytical expressions[45–47]. In this paper, we adopt the method in the Ref.[45] to obtain the QD of the two-point lattice, we will not given the analytical expression here, because the form is complicated. Then the QD is obtained between two end sites on the fractal lattices (given in Refs.[48–50]) by implementing the decimation RG method.

Fig. 7 shows the QDs versus anisotropy parameter  $\Delta$  and the temperature  $T$  (with the unit  $|J|/k_B$ ) in system A containing  $L$  sites. The variation trend of the QD between two end spins with temperature  $T$  is shown in Figs. 7(a) and (b). It can be seen that the QD exists maximum at  $T = 0$  and decreases with the increase of  $k_B T/|J|$ ; the thermal QD decreases with the increase of  $L$ , and it is almost zero at  $L \geq 30$ . From Figs. 7(c) and (d) we can find that the QD decreases with the increase of  $\Delta$ , no matter how large the size of system is, QD will change to 0 when  $\Delta = 1$ . And with the increase of  $L$ , the QD is smaller and smaller. Fig. 8 shows a sequential change of QD with anisotropy parameter  $\Delta$  and the temperature  $T$ . We can find that for  $L = 2$  case, there are a certain mutation in the contour at  $\Delta = 0$ ; For  $L > 2$  case, the QD first increase and then decrease to the special extremum values at  $\Delta = 0$  which is an unstable fixed point, where there exists the cusp of QD.

Fig. 9 and Fig. 10 show the QDs versus anisotropy parameter  $\Delta$  and the temperature  $T$  in system B and C. Their basic rule is similar to system A, but we find that there is a turning point at  $\Delta = 0$  by the calculation results. When  $\Delta > 0$  and  $T$  is zero or lower, the QD is reduced in turn with the increase of  $L$  until  $L \geq 684$ , there exists almost no QD; When  $\Delta \leq 0$  and  $T$  is zero or lower, the QD of  $L > 2$  exists a fixed value, which is consistent with the results in Figs. 9(a) and (b). Unlike system A, QD still exists when the the size of system is large ( $L = 2732$ ) in system B. From Figs. 9(c) and (d), we can find that the relation curve between QD and  $T$  no longer tends to smoothly decline when  $\Delta = 0$  which is an unstable fixed point, but there are a certain degree of twist. When  $\Delta > 0$ , the system

tends to be the Ising model, it tend to XY model when  $\Delta < 0$ . As shown in Fig. 10, in system C not only there are a certain degree of twist but also there is a cross point of the relation curve between QD and  $T$  at  $\Delta = 0$ , the degree of twist gradually increases with the increase of  $L$ . In order to further study the relation of QD with  $T$  and  $\Delta$ , we prepare the contour plots of QD on system B (Fig. 11) and C (Fig. 12), which show a sequential change of QD with  $\Delta$  and  $T$ . We can find that for  $L = 2$  case, there are a certain mutation in the contour at  $\Delta = 0$ ; For  $L > 2$  case, there exists the cusp of QD at  $\Delta = 0$ , in other words, the QD first increase and then decrease at this point.  $\Delta = 0$  is a critical point, from these we can easily find that QD can characterize quantum phase transitions of DH lattices effectively to a certain extent.

## V. THE QUANTUM EFFECT

In this section, we discuss the effect of quantum fluctuation and analyze the approximation which is induced by the noncommutativity. This effect has been examined by Takano and Suzuki [51], who have analyzed the discrepancy existing between the exact result and the approximate one. We note that, if we deal with a classical system on a linear chain, the exact solution corresponding to the entire chain can be straightforwardly achieved by solving finite pieces of the same chain. However, for quantum systems, it cannot be solved by such simplifying process because of the noncommutativity between the Hamiltonian of the finite pieces. In the following, we take system A as an example to discuss this effect. Firstly, we assume the generator of system A (Fig. 2(a1)) as the whole system that we will calculate. In this case, there will be no noncommutative effect and the rigorous result can be obtained as  $(K'(K, \Delta), \Delta'(K, \Delta))$ . For the same system, we apply the Migdal-Kadanoff method and obtain the approximative result which is defined as  $(2K''(K, \Delta; K, \Delta; K, \Delta), \Delta''(K, \Delta; K, \Delta; K, \Delta))$ . Finally, using the convenient ratios proposed in Ref. [36], we define the errors as

$$E^K \equiv \frac{2K''(K, \Delta; K, \Delta; K, \Delta)}{K'(K, \Delta)} - 1, \quad (20)$$

$$E^\Delta \equiv \frac{\Delta''(K, \Delta; K, \Delta; K, \Delta)}{\Delta'(K, \Delta)} - 1. \quad (21)$$

The  $T$ -dependence of  $E_F^K$  (for the F case) and  $E_{AF}^K$  (for the AF case) for typical values of  $\Delta$  is presented in Fig. 13. As we can see, both  $E_F^K$  and  $E_{AF}^K$  tend to zero in the  $T \rightarrow \infty$  limit,

and in the Ising limit ( $\Delta=1$ ), both  $E_F^K$  and  $E_{AF}^K$  equals zero at all temperatures. In the range of low temperatures, the fluctuation of the AF system is stronger than that of the F system which is in accordance with the previous conclusion [52]. With the decrease of  $\Delta$ , the effect of the fluctuation will be strengthened for both F and AF systems. The ordering is destroyed by the quantum fluctuation and this fact is responsible for the reentrant behavior in the phase diagram of system A. Furthermore, the competition between the quantum fluctuation and the thermal one is very important. At finite temperature, quantum fluctuation is usually suppressed in comparison with thermal fluctuation. However, when the temperature is close to zero, the quantum fluctuation dominate and strongly influence the critical behavior of the system. For systems B and C, we analyze the phase diagrams and consider that when the Néel temperature is relatively high, i.e., the thermal fluctuation dominate, the ordering will not be destroyed and there exists phase transition when  $\Delta$  is close to zero.

## VI. SUMMARY

We investigate the criticality of the spin-1/2 anisotropic AF Heisenberg model on the DH systems A, B and C, and obtain the phase diagrams and QD. For system A with  $d_f = 1.63$ , using the renormalization group approach straightforwardly, we find the reentrant behavior in the critical line and our results also show that  $T_c \sim \Delta$  when  $\Delta$  is close to zero. Moreover, we apply an effective combination method to study the phase diagrams of systems B and C (with  $d_f = 2$  and 2.58, respectively). The results show that the Néel temperature of system B tend to zero in the  $\Delta \rightarrow 0$  limit. On the other hand, if we consider the same  $J$  for both F and AF systems, the Néel temperature of system B is bigger than that of system C for the same values of  $\Delta$  and there exists phase transition in the isotropic Heisenberg model on system C. We also find that the thermal QC decreases with the increase of  $L$ , and the thermal correlation is almost zero in system A when  $L$  is large. For system B and system C, this is similar to system A when  $\Delta > 0$ , but QD exists when the the size of system is large and  $\Delta < 0$ . And there is a certain degree of twist of the relation curve between QD and  $T$  in system B and system C when  $\Delta = 0$ , we suspect that this may be related to their unstable fixed point. In the end, as an example, we discussed the quantum fluctuation of system A and our results indicate that, for low dimensional lattice, the fluctuation strongly influence the critical behavior of the AF system when  $T \rightarrow 0$ .

## Acknowledgments

This work is supported by the National Natural Science Foundation of China under Grants No. 11675090, No. 11847086, and No. 11905095; the Shandong Natural Science Foundation under Grant No. ZR2019PA015. P.-P.Z. would like to thank Rong-Tao Zhang, Zhe Wang, Pan-Pan Fang, Qi-Ming Wang, Li-Yuan Wang, Yue Li, Hai-Jun Ma, and Li-Dong Xiao for fruitful discussions and useful comments.

- 
- [1] Y. Gefen, B. B. Mandelbrot, A. Aharony, *Phys. Rev. Lett.* **45**, 855 (1980).
  - [2] Y. Gefen, A. Aharony, B. B. Mandelbrot, *J. Phys. A: Math. Gene.* **16**, 1267 (1983).
  - [3] Y. Qin, and Z. R. Yang, *Phys. Rev. B* **43**, 8576 (1991).
  - [4] A. O. Caride, C. Tsallis, and S. I. Zanette, *Phys. Rev. Lett.* **51**, 145 (1983).
  - [5] J. Ricardo de Sousa, N. S. Branco, B. Boechat, C. Cordeiro, *Physica A* **328** 167 (2003).
  - [6] S. N. Kempkes, M. R. Slot, S. E. Freeney, S. J. M. Zevenhuizen, D. Vanmaekelbergh, I. Swart and C. Morais Smith, *Nat. Phys.* **15**, 127 (2018).
  - [7] N. D. Mermin, H. Wagner, *Phys. Rev. Lett.* **17**, 1133 (1966).
  - [8] J. Ricardo de Sousa, *Physica A* **259** 138 (1998).
  - [9] R. Chitra, S. Pati, H. R. Krishnamurthy, D. Sen, and S. Ramasesha, *Phys. Rev. B* **52**, 6581 (1995).
  - [10] N. S. Branco and J. Ricardo de Sousa, *Phys. Rev. B* **62**, 5742 (2000).
  - [11] J. Ricardo de Sousa, and I. G. Araujo, *Phys. Lett. A* **272**, 333 (2000).
  - [12] I. G. Araujo, J. Ricardo de Sousa, and N. S. Branco, *Physica A* **305**, 585 (2002).
  - [13] P. J. Jensen, K. H. Bennemann, D. K. Morr and H. Dreyssé, *Phys. Rev. B* **73**, 144405 (2006).
  - [14] R. P. Singh, Z. C. Tao, and M. Singh, *Phys. Rev. B* **46**, 1244 (1992).
  - [15] C. M. Soukoulis, S. Datta, and Y. H. Lee, *Phys. Rev. B* **44**, 446 (1991).
  - [16] A. Cuccoli, T. Roscilde, V. Tognetti, R. Vaia and P. Verrucchi, *Phys. Rev. B* **67**, 104414 (2003).
  - [17] T. Krokhumalskii, V. Baliha, O. Derzhko, J. Schulenburg, and J. Richter, *Phys. Rev. B* **95**, 094419 (2017).
  - [18] J. Ricardo de Sousa and J. A. Plascak, *Phys. Lett. A* **237**, 66 (1997).

- [19] B. G. Liu, Phys. Rev. B **41**, 9563 (1990).
- [20] J. Ricardo. de Sousa and I. G. Araújo, Solid State Commun. **115**, 265 (2000).
- [21] T. Roscilde, A. Cuccoli, and P. Verrucchi, physica status solidi (b) **236**, 433 (2004).
- [22] C. H. Bennett, G. Brassard, C. Crépeau, R. Jozsa, A. Peres, and W. K. Wootters, Phys. Rev. Lett. **70**, 1895 (1993).
- [23] A. Niezgoda, M. Panfil, and J. Chwedeńczuk, Phys. Rev. A **102**, 042206 (2020).
- [24] A. Szasz, Phys. Rev. A **99**, 062313 (2019).
- [25] S. Siwiak-Jaszek, T. P. Le, and A. Olaya-Castro, Phys. Rev. A **102**, 032414 (2020).
- [26] H. Ollivier and W. H. Zurek, Phys. Rev. Lett. **88**, 017901 (2001).
- [27] L. Henderson and V. Vedral, J. Phys. A: Math. Gen. **34**, 6899 (2001).
- [28] K. Modi, A. Brodutch, H. Cable, T. Paterek, and V. Vedral, Rev. Mod. Phys. **84**, 1655 (2012).
- [29] Y. L. Xu, X. Zhang, Z. Q. Liu, X. M. Kong, and T. Qi, Ren Eur. Phys. J. B **87**, 132 (2014).
- [30] G. Adesso, T. R. Bromley, and M. Cianciaruso, J. Phys. A: Math. Theor. **49**, 473001 (2016).
- [31] F. G. S. L. Brandão, M. Piani, and P. Horodecki, Nat. Commun. **6**, 7908 (2015).
- [32] V. Madhok and A. Datta, Int. J. Mod. Phys. B **27**, 1345041 (2013).
- [33] D. Girolami, A. M. Souza, V. Giovannetti, T. Tufarelli, J. G. Filgueiras, R. S. Sarthour, D. O. Soares-Pinto, I. S. Oliveira, and G. Adesso, Phys. Rev. Lett. **112**, 210401 (2014).
- [34] K. Brádler, M. M. Wilde, S. Vinjanampathy, D. B. Uskov, Phys. Rev. A **82**, 062310 (2010).
- [35] M. Usman, K. Khan, The European Physical Journal D **74**, 181 (2020).
- [36] A. M. Mariz, C. Tsallis, and A. O. Caride, J. Phys. C **18**, 4189 (1985).
- [37] Z. R. Yang, Phys. Rev. B **38**, 728 (1988).
- [38] X. M. Kong and Z. R. Yang, Phys. Rev. E **69**, 016101 (2004).
- [39] N. D. Mermin and H. Wagner, Phys. Rev. Lett. **17**, 1133 (1966).
- [40] S. S. Aplesnin, J. Phys: Condens. Mat. **10**, 10061 (1998).
- [41] W. G. Clark and L. C. Tippie, Phys. Rev. B **20**, 2914 (1979).
- [42] J. Ricardo de Sousa, Phys. Lett. A **216**, 321 (1996).
- [43] B. Groisman, S. Popescu, and A. Winter, Phys. Rev. A **72**, 032317 (2005).
- [44] B. Schumacher and M. D. Westmoreland, Phys. Rev. A **74**, 042305 (2006).
- [45] M. Ali, A. R. P. Rau, and G. Alber, Phys. Rev. A **81**, 042105 (2010).
- [46] J. Maziero, T. Werlang, F. F. Fanchini, L. C. Céleri, R.M. Serra, Phys. Rev. A **81**, 022116 (2010).

- [47] Q. Chen, C. Zhang, S. Yu, X. X. Yi, C. H. Oh, Phys. Rev. A **84**, 042313 (2011).
- [48] A. N. Berker, S. Ostlund, J. Phys.: Condens. Matter **12**, 4961 (1979).
- [49] R. B. Griffiths, M. Kaufman, Phys. Rev. B **26**, 5022 (1982).
- [50] M. Kaufman, R.B. Griffiths, Phys. Rev. B **30**, 244 (1984).
- [51] H. Takano and M. Suzuki, J. Stat. Phys **26**, 635 (1981).
- [52] J. Fröhlich and E. H. Lieb, Phys. Rev. Lett. **38**, 440 (1977).
- [53] J. Hove, and A. Sudbø, Phys. Rev. B **75**, 104405 (2007).

## Figure Captions

Fig. 1 The structure of three DH lattices.  $P$  denotes the number of branches and  $L$  denotes the number of bonds per branch. They all start from a two-point lattice and generate the lattices from the middle generators in an iterative manner.

Fig. 2 Self-dual two-terminal clusters used in the RG transformation. (a) System A. (a1) Cluster that generates, through six interactions. (a2) The renormalized two-site cluster. (b) System B. (b1) The third step in the construction of the 2D antiferromagnetic DH lattice. (b2) Cluster that generates, through four interactions. (b3) Two-site cluster. The first step from (b1) to (b2) is the equivalent transformation and the second step is the renormalization group transformation.

Fig. 3 Phase diagrams of the Heisenberg AF and F models on system A. The red line correspond to the AF anisotropic Heisenberg model and the inset shows the phase diagram of F anisotropic Heisenberg models. O(D) stands for ordered (disordered) phase. The open circle and the full square denote the semistable and fully stable fixed points, respectively.

Fig. 4 The critical temperature behaves of system A. (a) and (b) respect the critical temperature  $T_c$  of F case and the Néel temperature  $T_N$  of AF varies with  $\Delta$ , respectively.

Fig. 5 Phase diagrams of the AF Heisenberg model on systems B and C, and the phase diagram on system A is also depicted for comparison. There exists a reentrant behavior in system A, the Néel temperature tends to zero when decreasing  $\Delta$  in system B and there exists phase transition in the isotropic Heisenberg limit  $\Delta = 0$  in system C.

Fig. 6 The critical temperature behaves of system B for low temperatures in the  $\Delta \rightarrow 0$  limit in AF case. The Néel temperature  $T_N$  is directly proportional to  $\ln \Delta$ .

Fig. 7 The QD between two end spins on system A with  $L$  site varies with  $T$  (with the unit  $|J|/k_B$ , the same below) and anisotropy parameter  $\Delta$ . (a) and (b) the QD varies with  $T$ , (c) and (d) the QD varies with  $\Delta$ . The QD curves for different  $L$  cases have a cross point and a certain degree of twist at  $\Delta = 0$ .

Fig. 8 The contour plots of QD on system A with  $L$  site varies with  $T$  and anisotropy parameter  $\Delta$ . The contour of QD for different  $L$  cases have a cross point and a certain degree of twist at  $\Delta = 0$ . When  $L = 2$ , there are a mutation in the contour of QD at  $\Delta = 0$ ; When  $L > 2$ , there exists the cusp in the contour of QD at  $\Delta = 0$ .

Fig. 9 The quantum discord between two end spins on system B with  $L$  site varies with with  $T$  and  $\Delta$ . (a) and (b) the QD varies with  $T$ , (c) and (d) the QD varies with  $\Delta$ . The QD curves for different  $L$  cases have a certain degree of twist at  $\Delta = 0$ .

Fig. 10 The quantum discord between two end spins on system B with  $L$  site varies with  $T$  and  $\Delta$ . (a) and (b) the QD varies with  $T$ , (c) and (d) the QD varies with  $\Delta$ . The QD curves for different  $L$  cases have a cross point and a certain degree of twist at  $\Delta = 0$ .

Fig. 11 The contour plots of QD on system B with  $L$  site varies with  $T$  and anisotropy parameter  $\Delta$ . The contour of QD for different  $L$  cases have a cross point and a certain degree of twist at  $\Delta = 0$ . When  $L = 2$ , there are a mutation in the contour of QD at  $\Delta = 0$ ; When  $L > 2$ , there exists the cusp in the contour of QD at  $\Delta = 0$ .

Fig. 12 The contour plots of QD on system C with  $L$  site varies with  $T$  and anisotropy parameter  $\Delta$ . The contour of QD for different  $L$  cases have a cross point and a certain degree of twist at  $\Delta = 0$ . When  $L = 2$ , there are a mutation in the contour of QD at  $\Delta = 0$ ; When  $L > 2$ , there exists the cusp in the contour of QD at  $\Delta = 0$ .

Fig. 13 Thermal dependence of the errors  $E_F^K$  and  $E_{AF}^K$  defined by Eq. (21), for typical values of  $\Delta$ . It can be seen obviously that the error for the F system are bigger than the AF system at low temperatures. Our calculation also shows  $E_F^K = E_{AF}^K = 0$  at the Ising limits ( $\Delta = 1$ ).

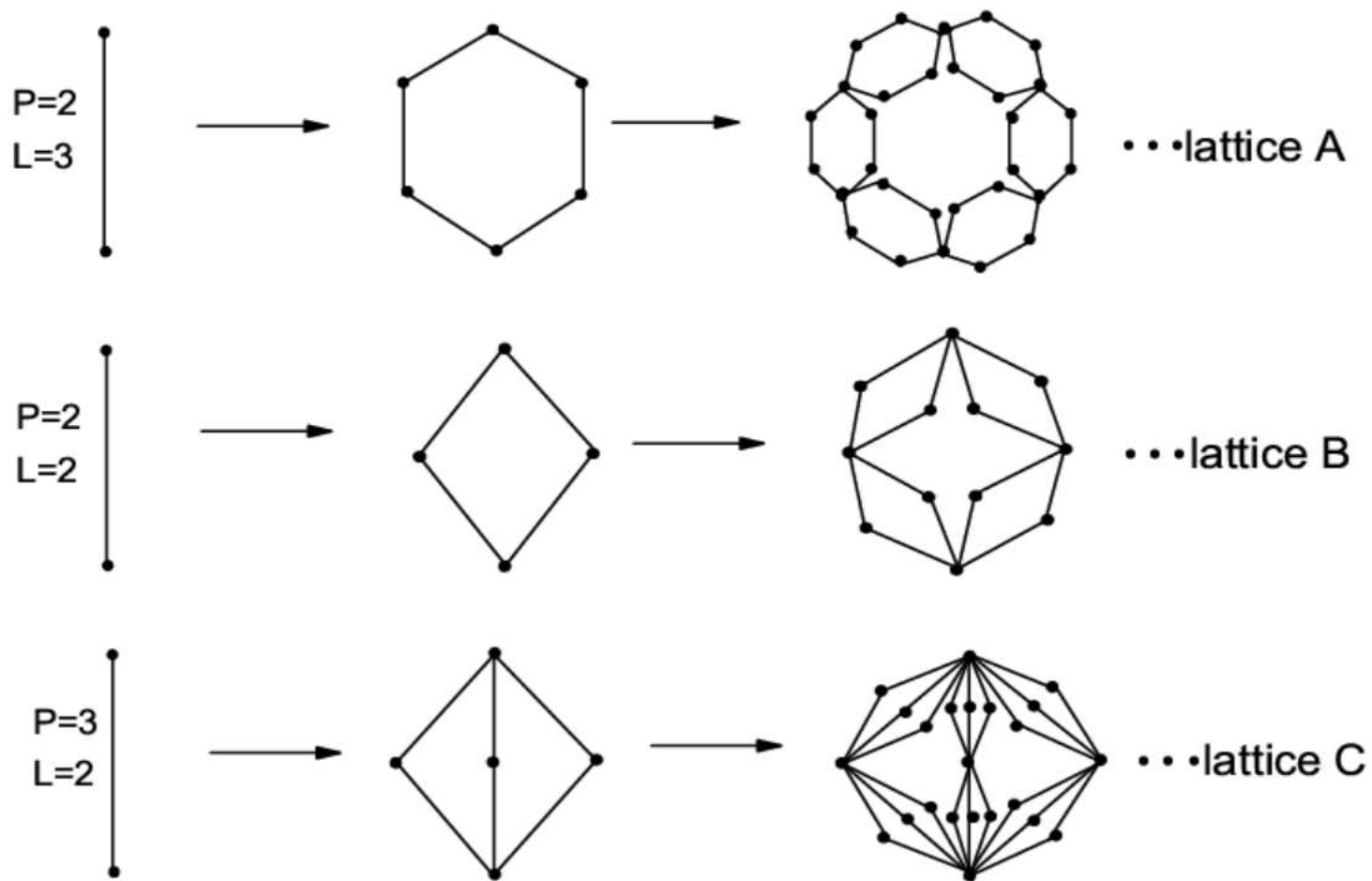


Fig. 1



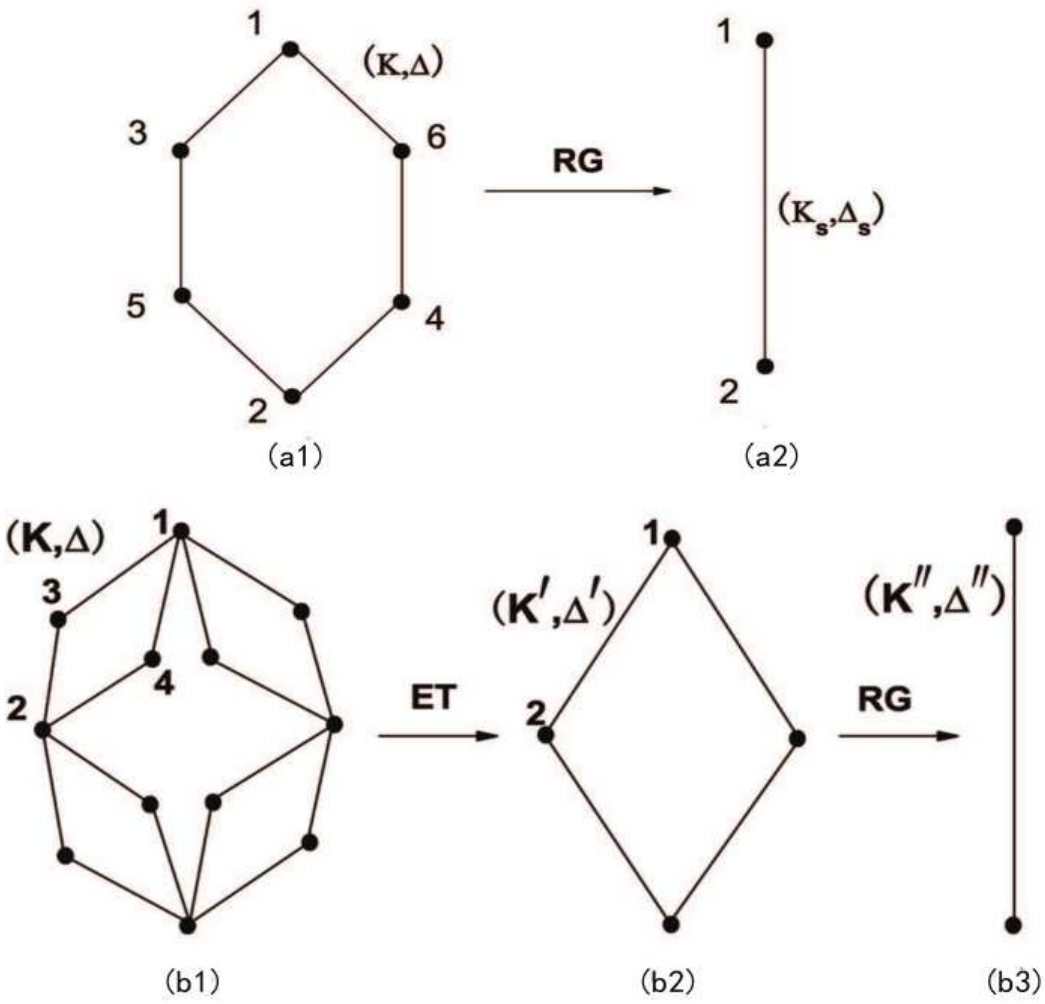


Fig. 2

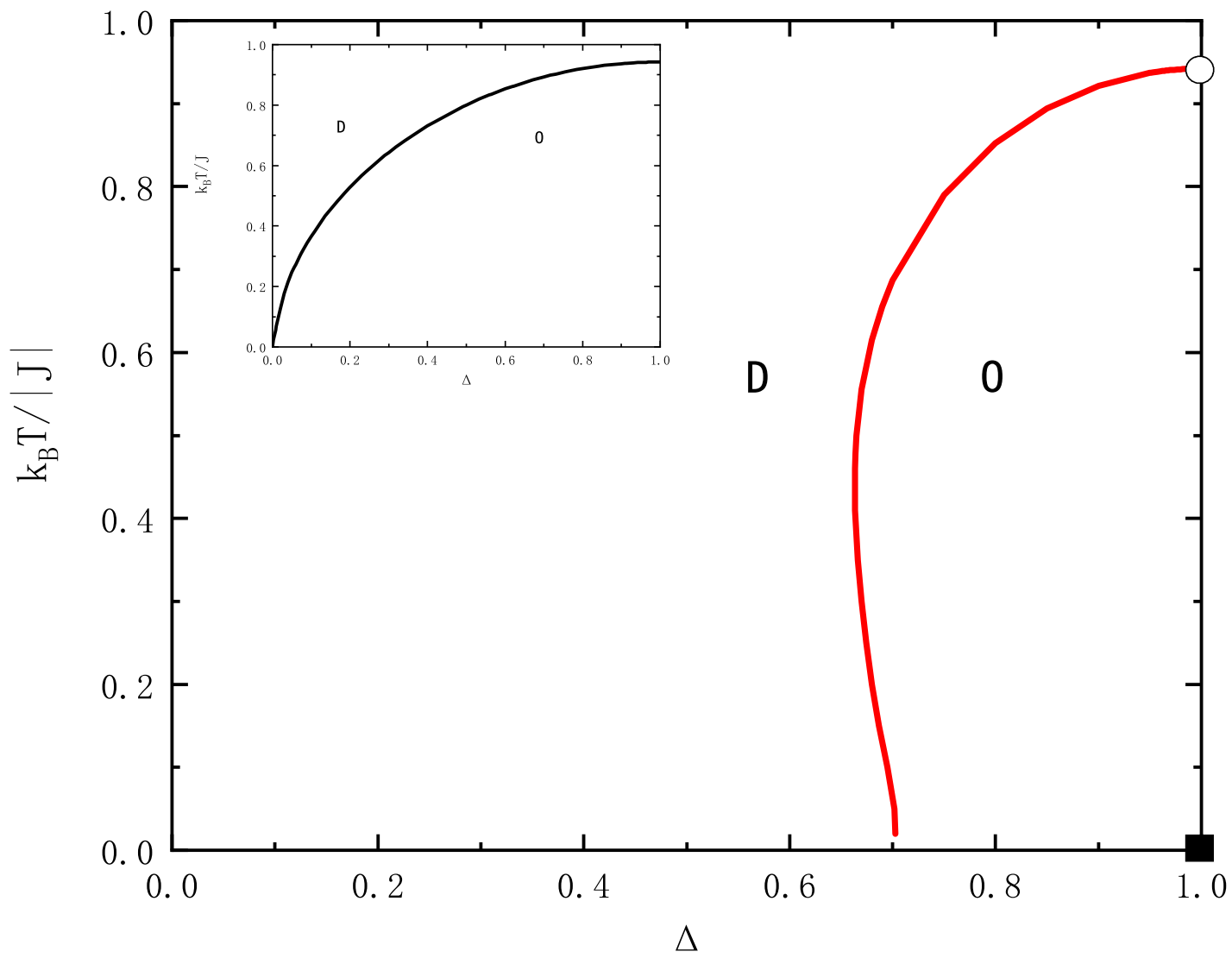


Fig. 3

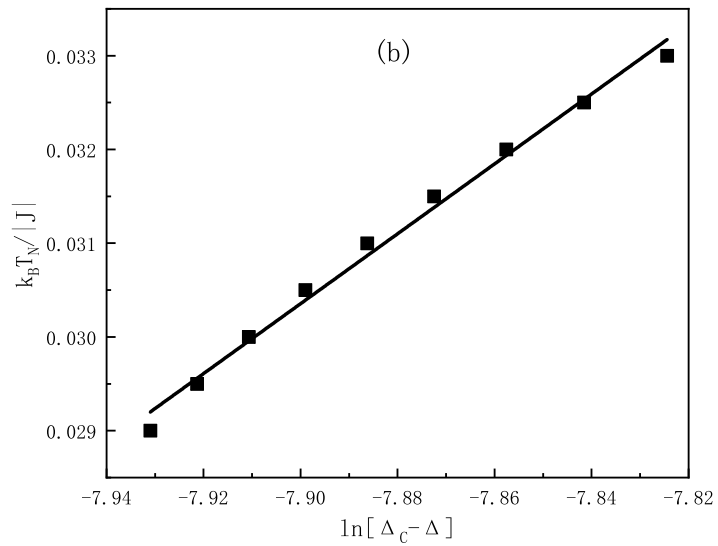
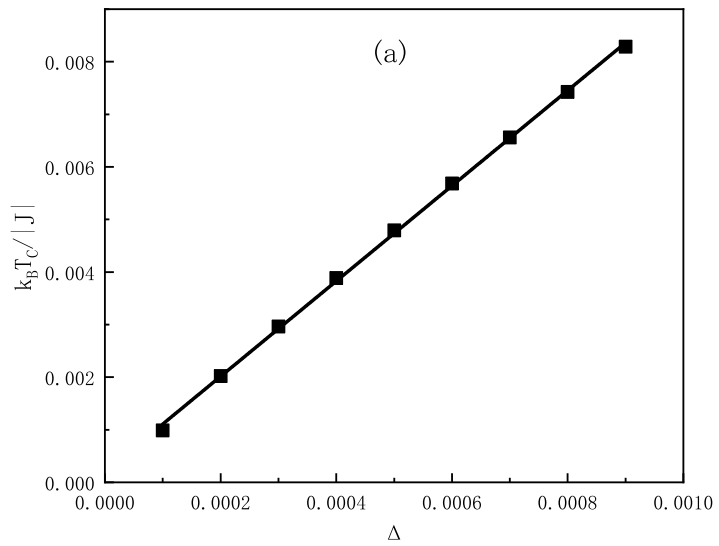


Fig. 4

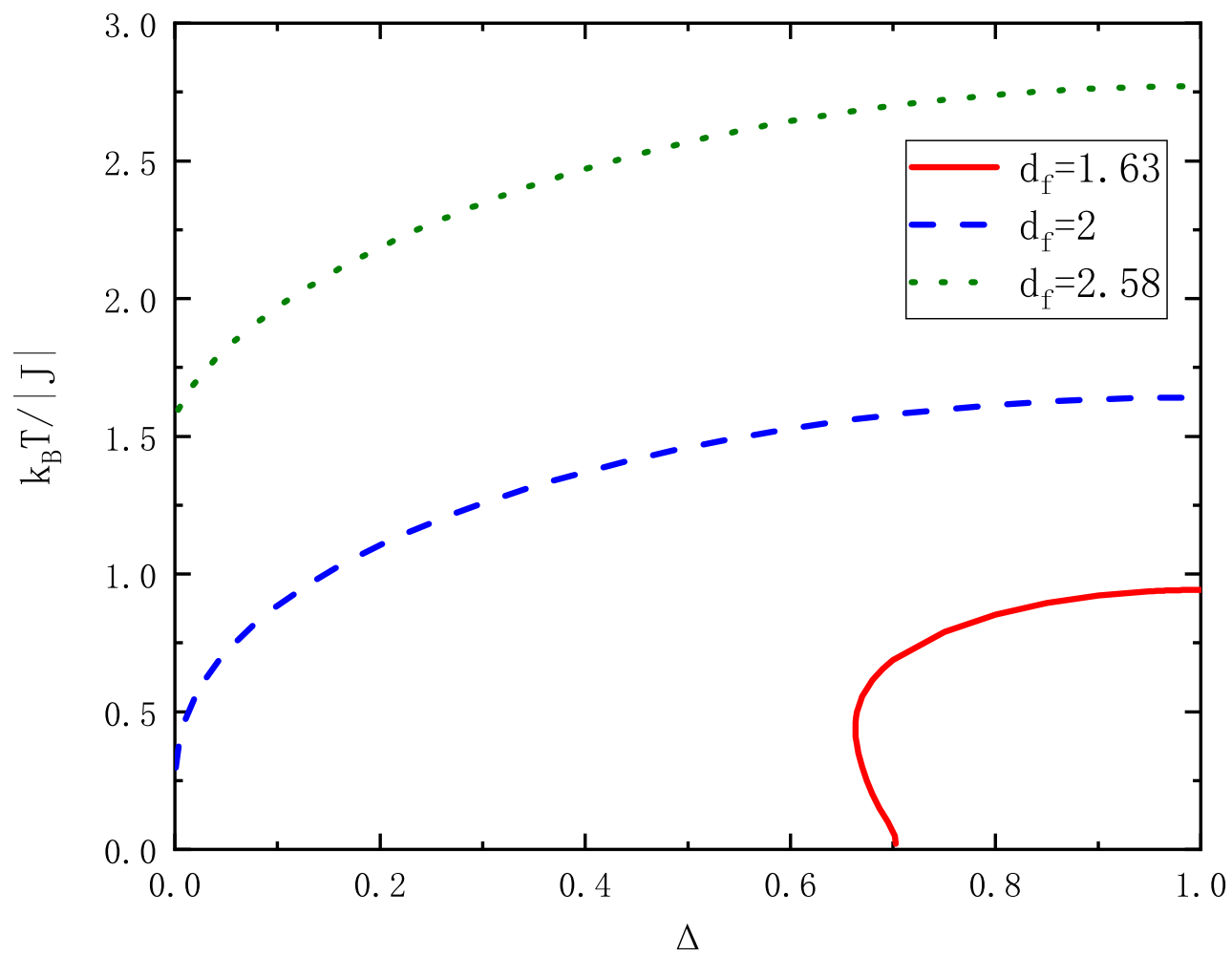


Fig. 5

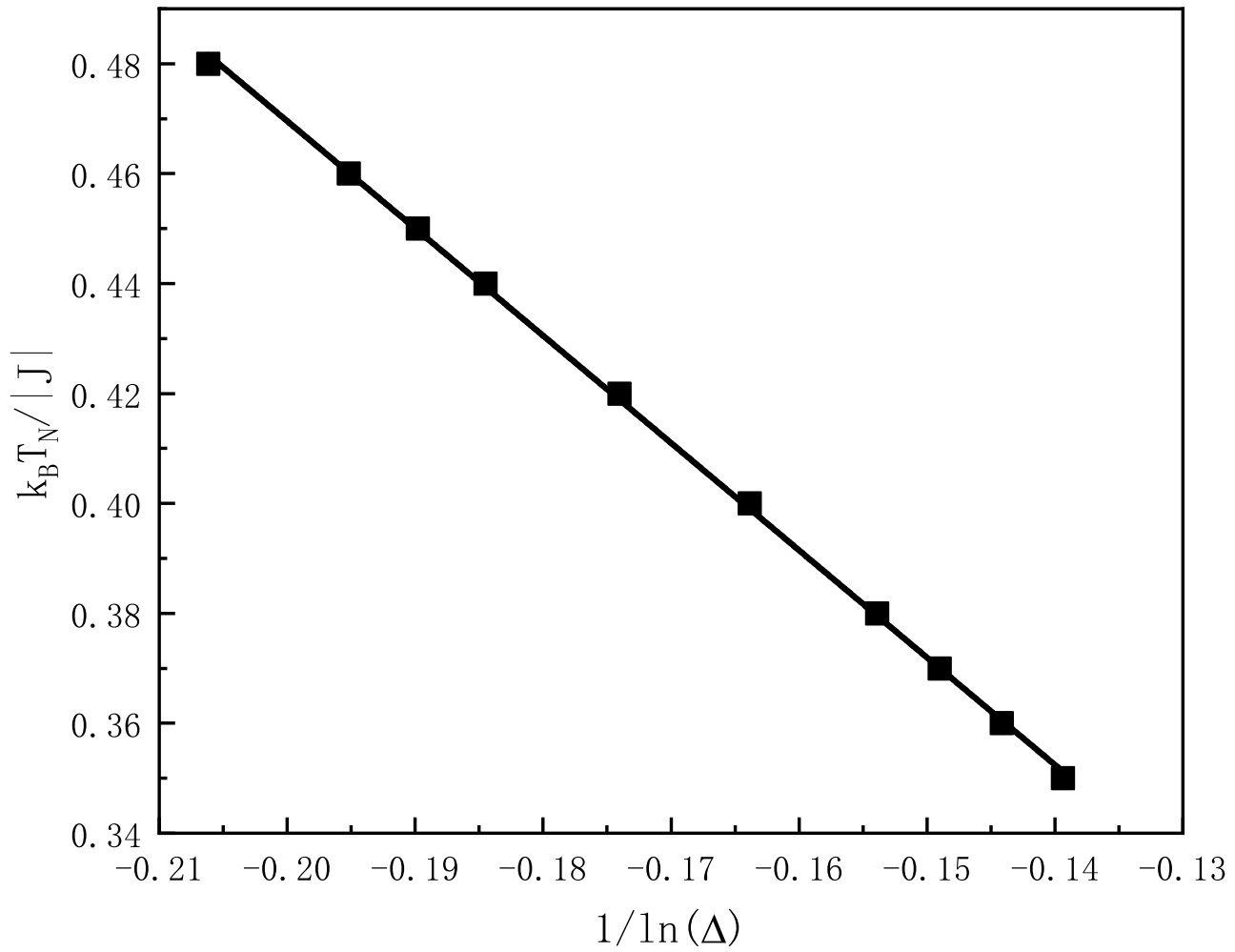


Fig. 6

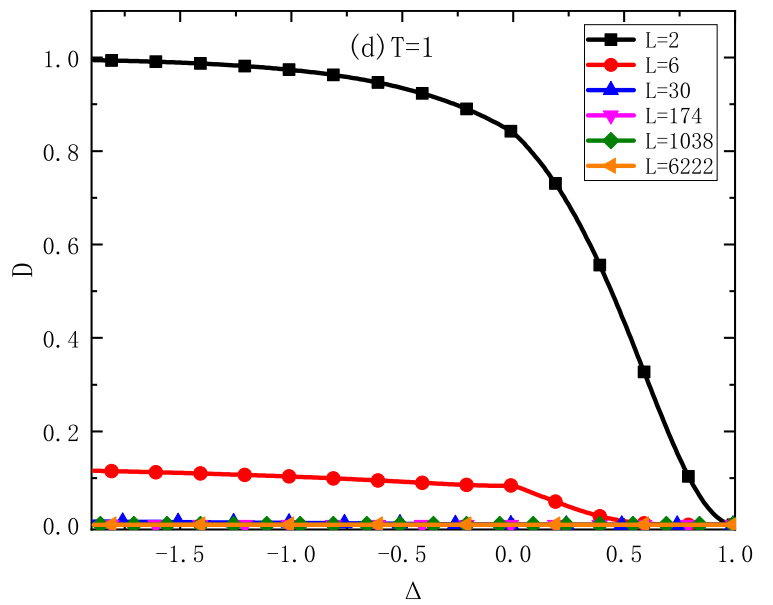
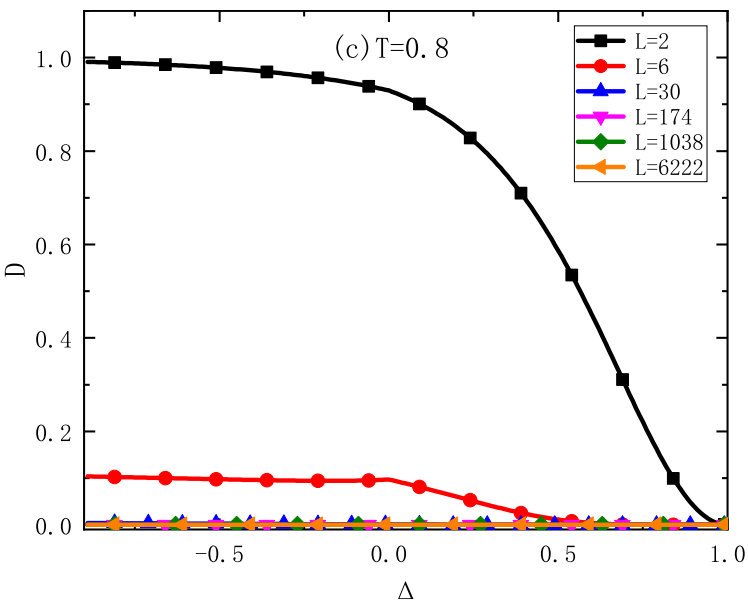
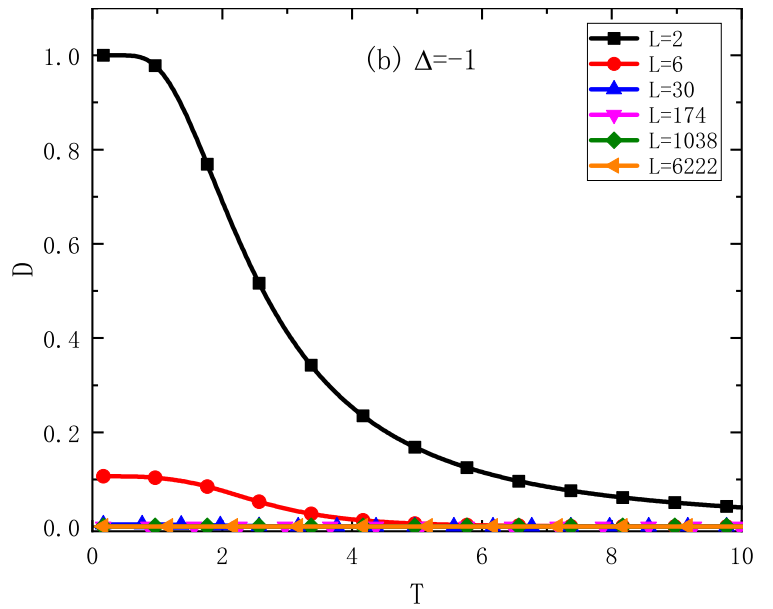
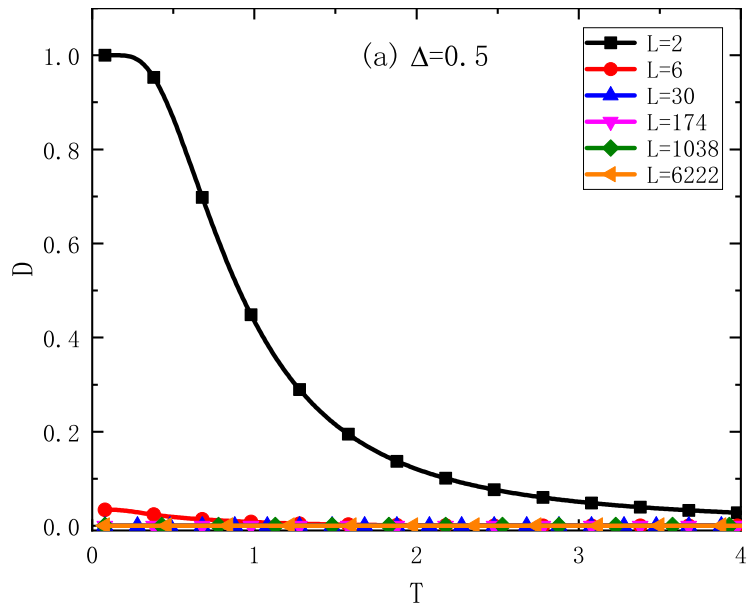


Fig. 7

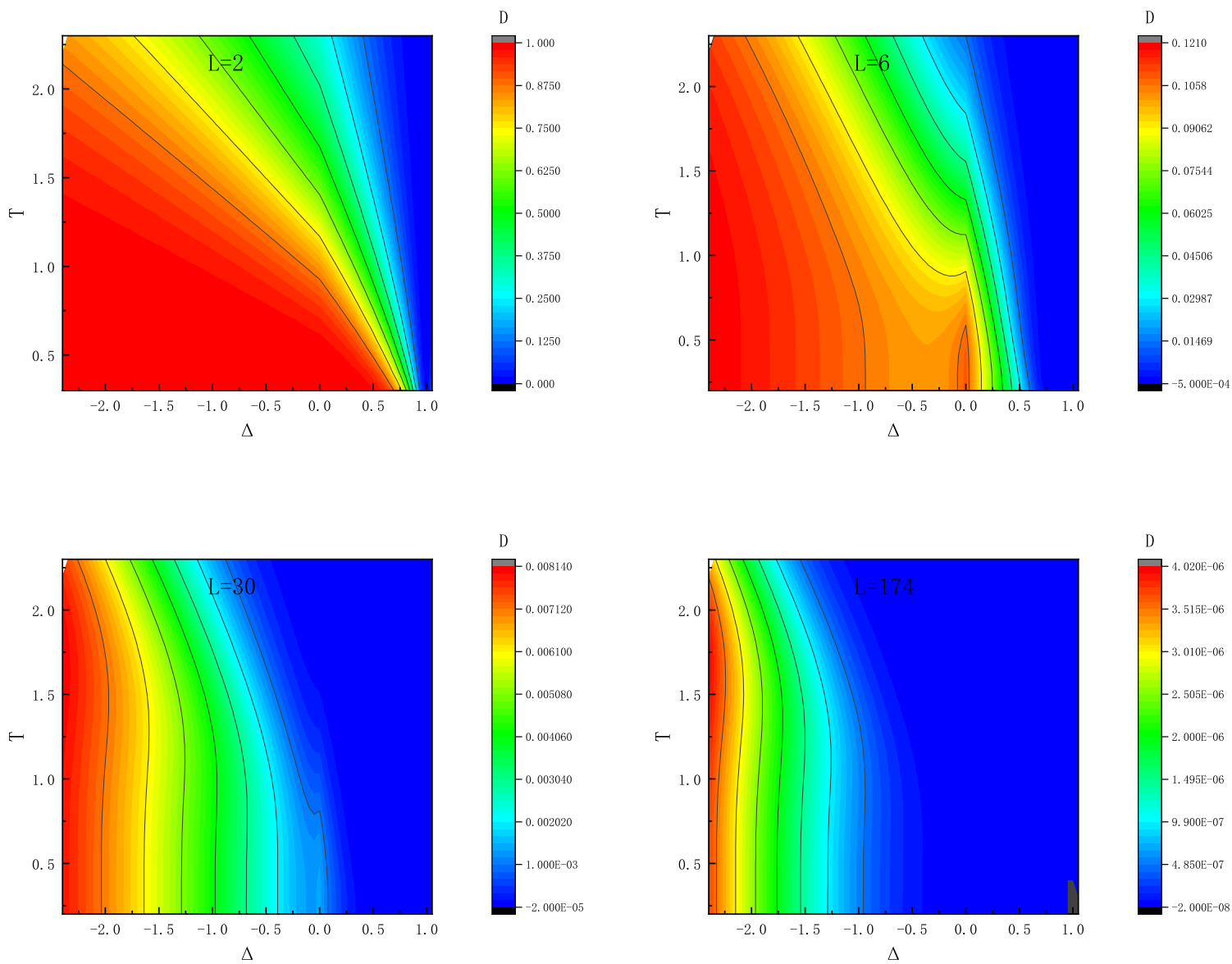


Fig. 8

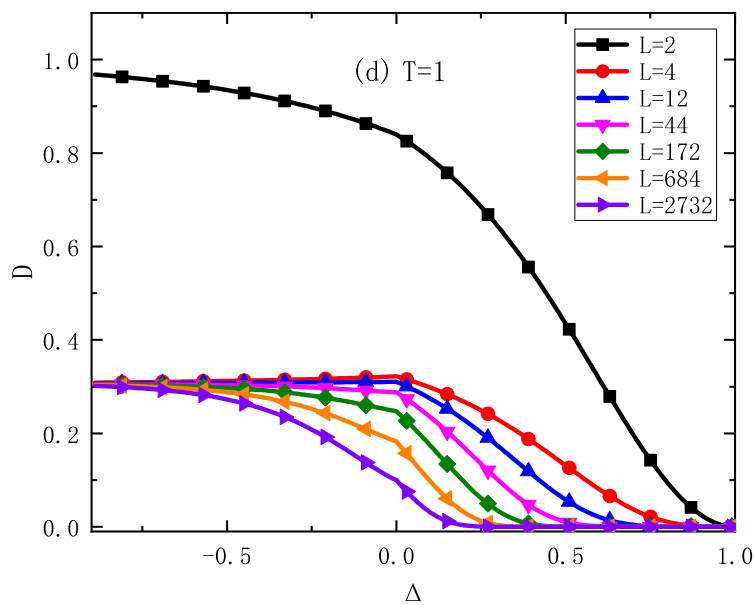
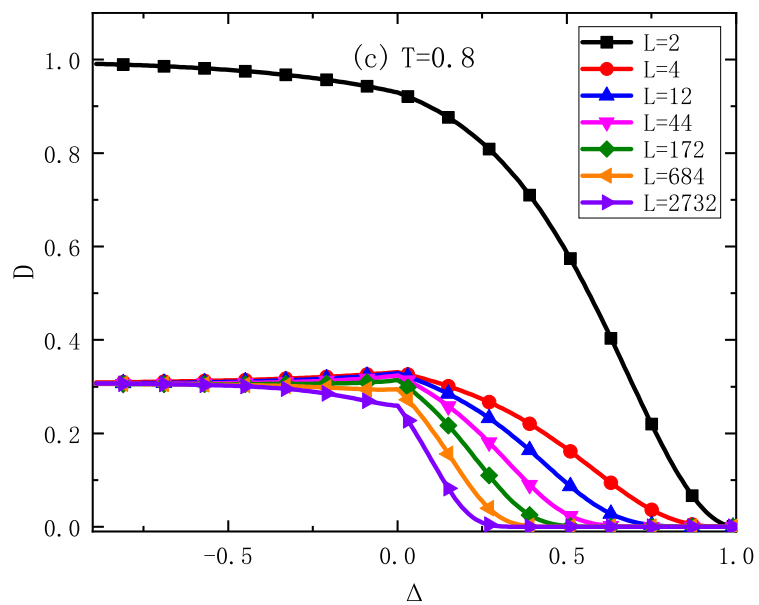
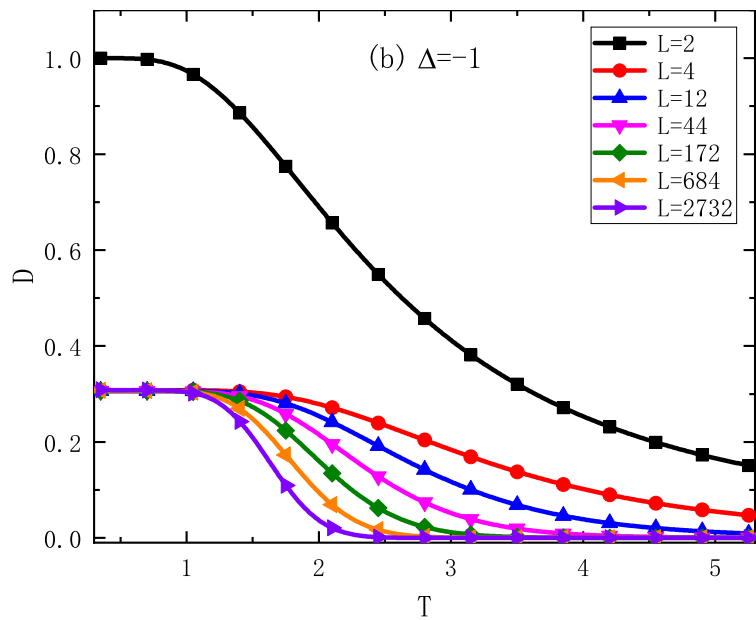
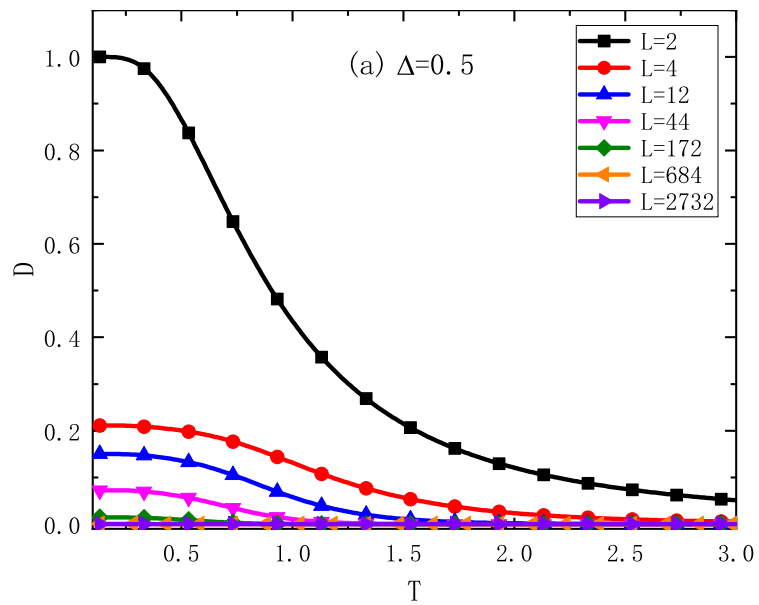


Fig. 9



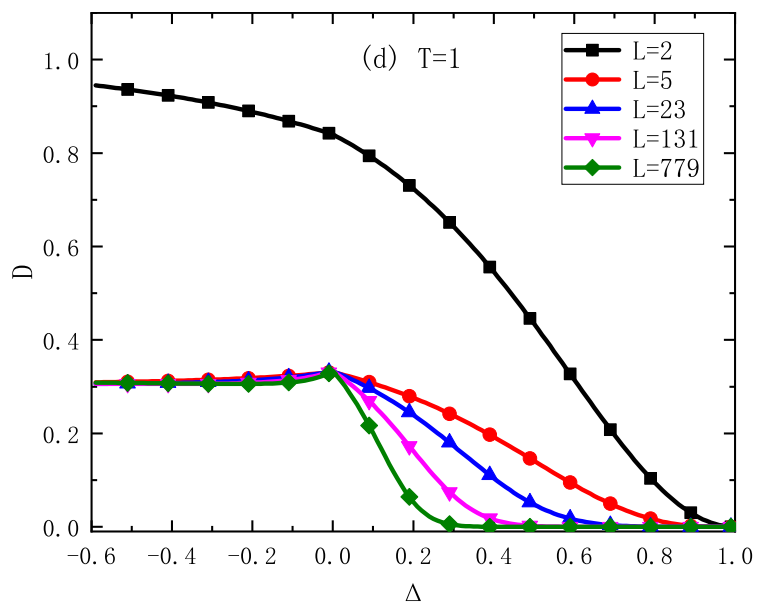
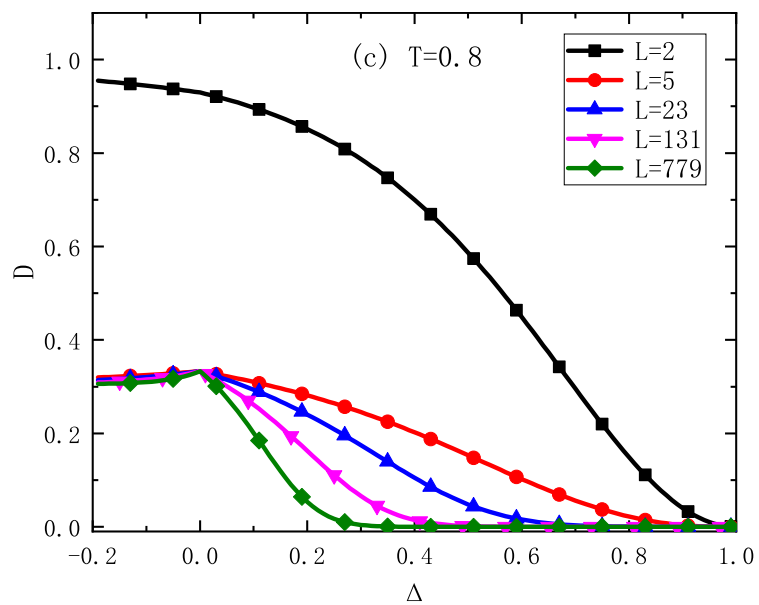
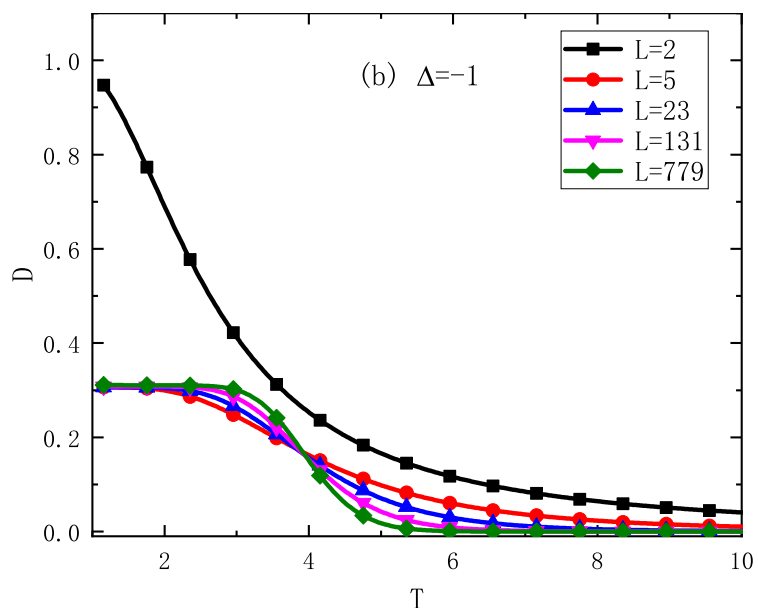
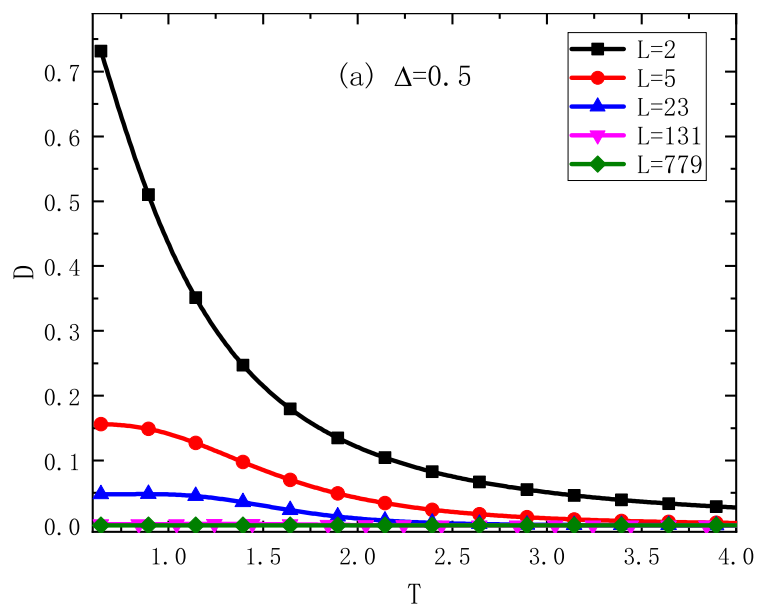


Fig. 10

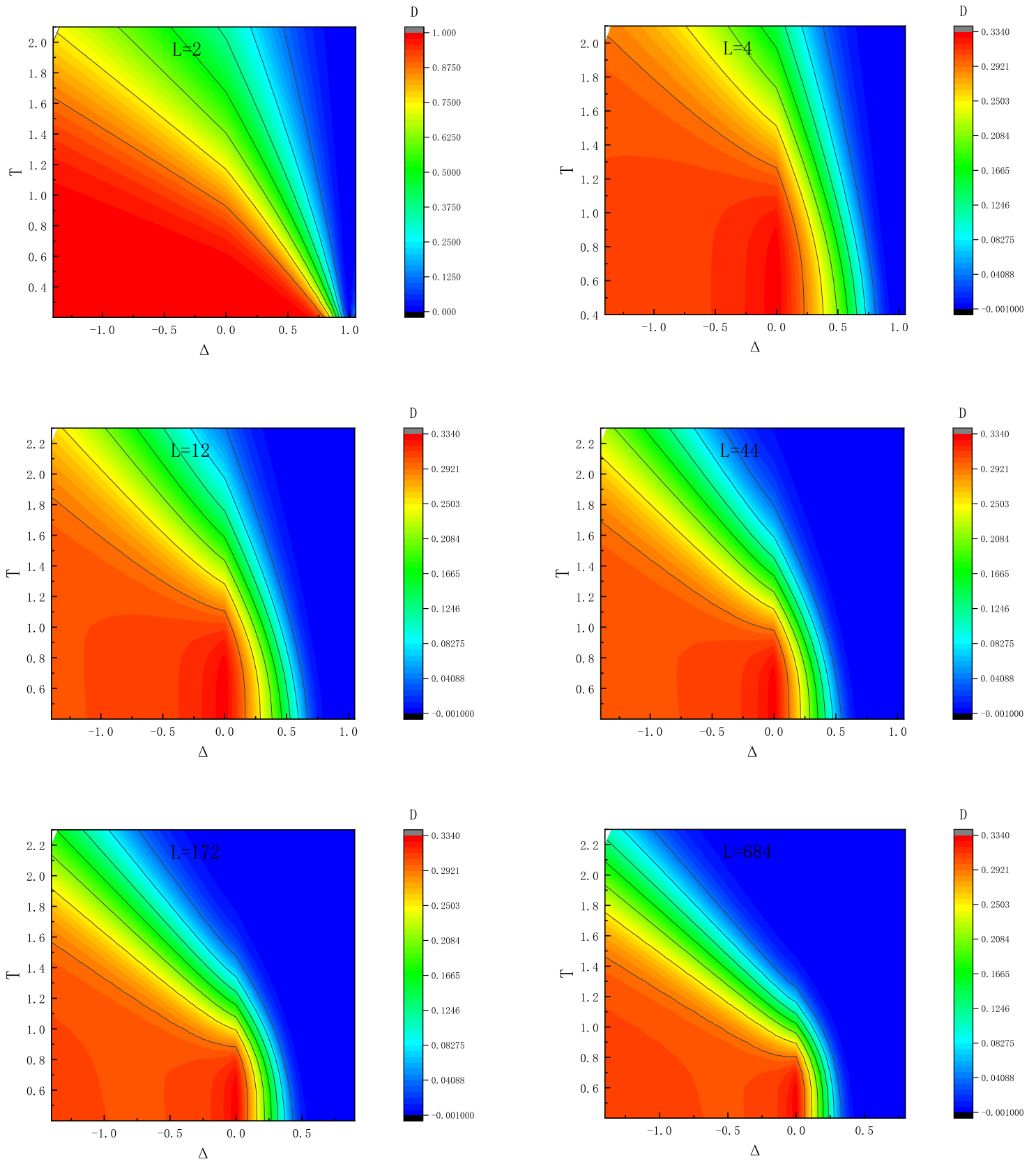


Fig. 11

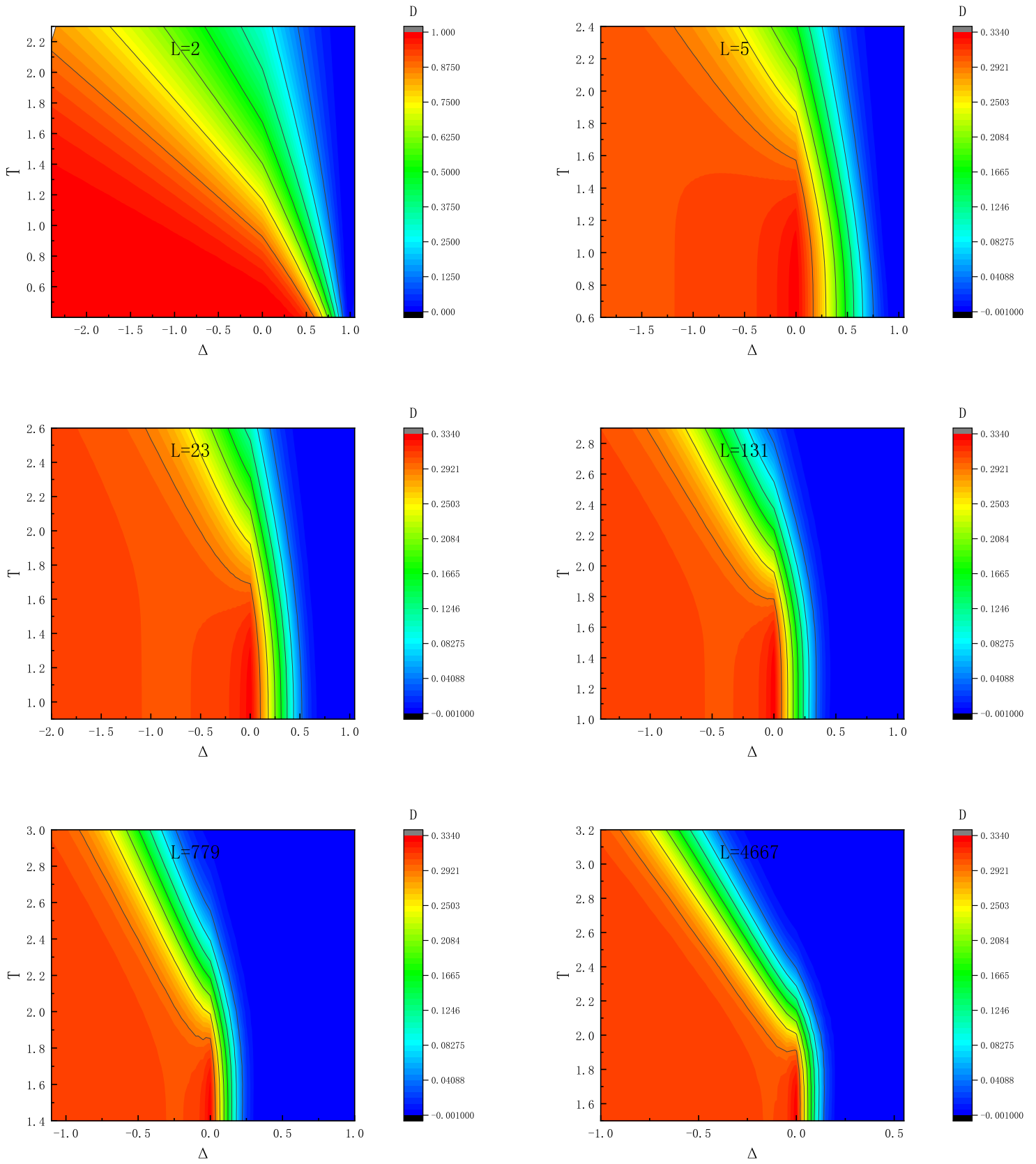


Fig. 12

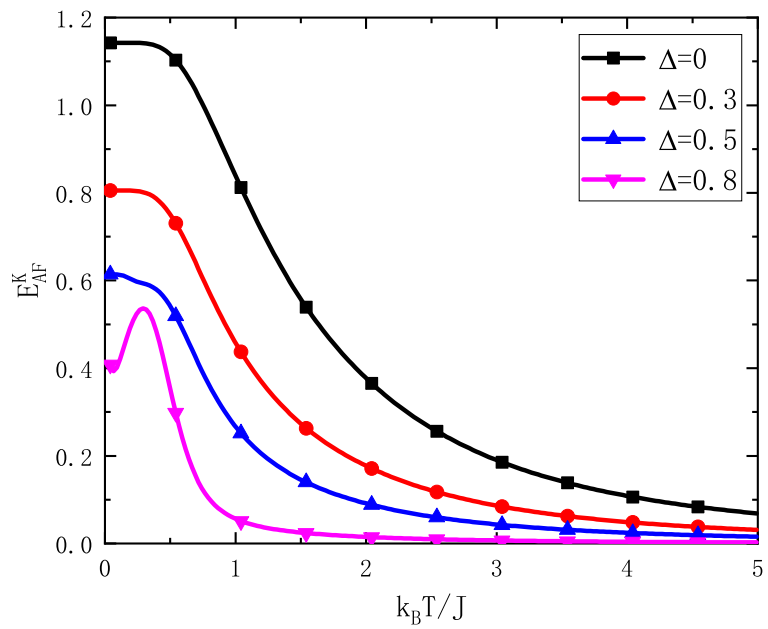
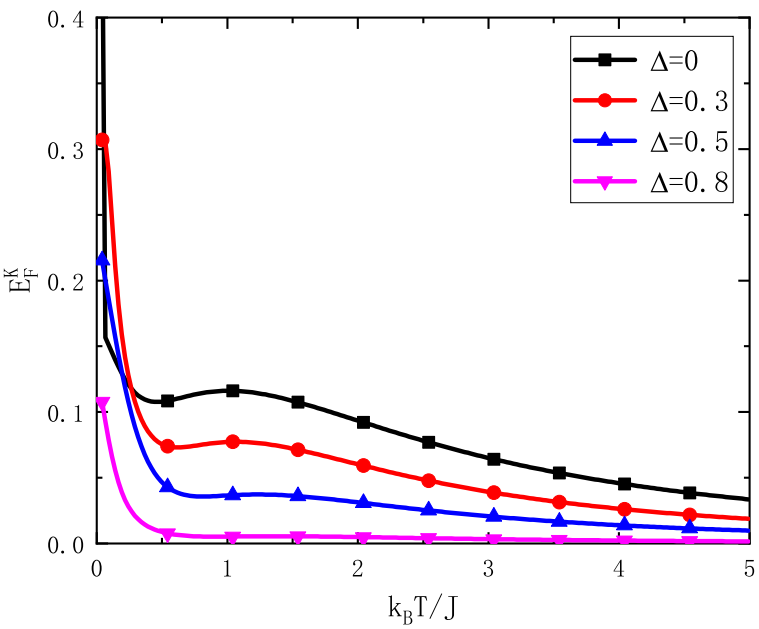


Fig. 13